I&EC research
Industrial & Engineering Chemistry Research

pubs.acs.org/IECR
Article

Thin-Film Catalysis Innovations in Fischer–Tropsch Synthesis for Enhanced Activity

Avela Kunene,* Yangjun Wei, Eric van Steen, Muhammad Hamid Raza, Imane El Arrouji, Catalina E. Jimenez, Roberto Félix, Daniel M. Toebbens, Ali Shan Malik, Veroushia Padayachee, Dominic De Oliveira, Mohamed Islam Fadlalla, Marcus Bär, Sonya Calnan, Michael Claeys, Rutger Schlatmann, and Daniel Amkreutz

Cite This: *Ind. Eng. Chem. Res.* 2025, 64, 22939–22948

Read Online

ACCESS | Metrics & More | Article Recommendations | Supporting Information

ABSTRACT: For 100 years, Fischer–Tropsch synthesis (FTS) technology has been underpinned by cobalt- and iron-based powder catalyst systems. Nevertheless, due to cost efficiency and lower material requirements, thin-film cobalt catalysts are currently being evaluated as an alternative to traditional powder catalysts. In this study, we explore the catalytic performance of the Co-SiO_x/Al thin-film catalyst under relevant FTS conditions. Thus, the cobalt active metal is deposited onto the aluminum foil substrate by magnetron sputtering. To avoid alloy formation between the cobalt and aluminum foil, the cobalt layer is supported by a SiO_x buffer layer deposited by plasma-enhanced chemical vapor deposition (PECVD). To evaluate the catalyst, the reduction of the cobalt moiety was assessed using in situ synchrotron grazing incident X-ray diffraction (GI-XRD) conducted at beamline KMC-2 at the BESSY II Light Source under flowing H_2 at 350 °C. Ultimately, the prepared thin film catalyst is tested for FTS at a total flow rate (H_2/CO = 2:1) of 40, 20, and 5 sccm under relevant FTS conditions. CO conversion levels of 0.9, 1.2, and 2.7% were achieved at 40, 20, and 5 sccm, respectively. The observed low CO conversion levels are ascribed to low cobalt loadings of the thin-film catalyst. Upon considering the cobalt loading, the corresponding rates of CO consumption ($-r_{CO}$) of 23, 40, and 61 $g_{CO}/g_{Co}/h$ were obtained at 40, 20, and 5 sccm, respectively. This highlights that the Co-SiO_x/Al thin-film catalyst performance is comparable and, in other cases, outperforms unpromoted Co-based powder catalysts.

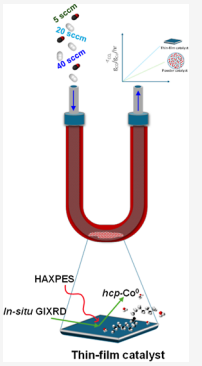

INTRODUCTION

Growing interest in higher molecular weight hydrocarbons Fischer–Tropsch (FT) waxes has emerged due to their potential applications in synthetic fuels[1] and lubricants.[2] These hydrocarbons are primarily produced from syngas (i.e., a gas mixture of H_2 and CO) through low-temperature FT synthesis (LTFTS), typically operating between 200 and 250 °C.[3,4] The development of an active and stable catalyst with a high FT wax selectivity is a crucial factor in advancing FT technology. Cobalt-based powder catalysts have been considered as one of the most favorable catalyst systems for the synthesis of long-chain hydrocarbons due to their high activity, high selectivity to linear paraffins, and low water–gas shift (WGS) activity.[5,6] However, the main limitation of the liquid-phase FTS reaction is the slow diffusion rate of the syngas and products inside the catalyst pores, which are filled with formed hydrocarbons and solvent.[7] This blockage of active catalytic sites ultimately hinders accurate measurement of the intrinsic catalytic activity during FTS, as it limits the accessibility of reactants to the catalyst surface and affects overall reaction kinetics.

Several solutions, e.g., transient processing by switching syngas to a H_2-rich feed gas for a pore-draining hydrogenolysis sequence[2,8] or bimodal pore structure for the powder catalyst to minimize mass transfer resistances and to facilitate liquid drainage[9] have been explored to prolong the catalyst lifetime, and are proposed in the literature.

In contrast to these conventional methods to "revive" the active sites, the concept of thin-film cobalt catalysts has emerged as an alternative approach to traditional powder catalysts for various reasons: Thin-film catalysts offer enormous potential for atomic-scale control of catalyst chemical composition and morphology and their supports, offering the advantage of tunable parameters (e.g., component gradient of active metals, microstructuring of bulk and surface materials, etc.) that can potentially improve catalytic performance as well as achieve economic upscaling.[10]

Although the application of thin-film catalysts on acetylene semihydrogenation[10,11] and methane dry reforming[10] has been reported in the literature, to our knowledge, the application of thin-film catalysts in FTS is in its early phase. This requires further investigation to fully understand the potential that

Received: July 3, 2025
Revised: November 10, 2025
Accepted: November 13, 2025
Published: November 19, 2025

https://doi.org/10.1021/acs.iecr.5c02728
Ind. Eng. Chem. Res. 2025, 64, 22939–22948

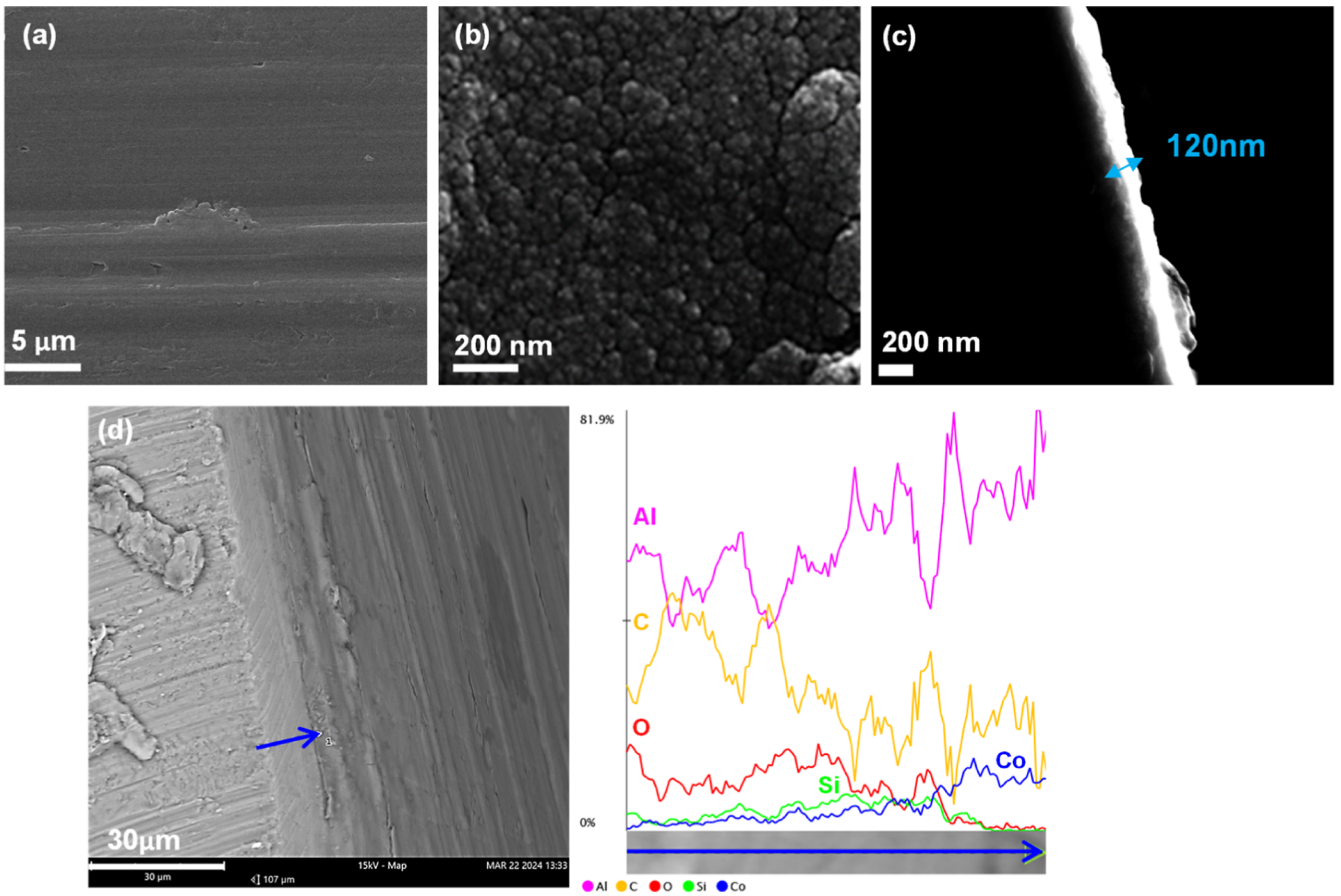

Figure 1. (a,b) SEM top-view images of a closed Co-SiO_x/Al thin-film catalyst, (c) cross-sectional image of the Co-SiO_x/Al thin film catalyst, and (d) cross-section EDX composition mapping of the Co-SiO_x/Al thin-film catalyst.

cobalt-based thin-film catalysts hold in FTS technology and, ultimately, optimize their performance. Nonetheless, the proposed thin-film approach could already highly favor FTS in several ways:

i FTS performance depends strongly on catalyst activity and selectivity, whereas catalyst design depends on material component and distribution and surface/bulk microstructuring, and nanoparticle dimensioning can hardly be achieved for powder-based catalysts but is achievable for thin-film approaches.

ii Precise control of the studied catalyst shall potentially shed more light on the chemical mechanism of the FTS process, and thin-film catalysts open a way for material exploration and catalyst characterization.[11]

iii Due to much lower catalyst loadings but significantly greater exposure of the active sites to the reactants, the thin-film catalysts may contribute to greater cost efficiency and lower material requirements—highly attractive qualities for upscaling applications.

In this study, we explore the FTS catalytic performance of a (0.07 wt %) Co-SiO_x/Al-based thin-film catalyst at various weight hourly space velocities and investigate the dynamics of the thin-film catalyst using reference samples deposited on fused silica wafers using in situ spectroscopy. The active cobalt metal is deposited in its metallic form onto an aluminum foil as a substrate using magnetron sputtering. The cobalt layer is further stabilized on the substrate by prior deposition of a SiO_x interlayer by plasma-enhanced chemical vapor deposition (PECVD). First, we investigate the chemical, morphological, and crystallographic properties of the thin-film catalyst using scanning electron microscopy with energy dispersive X-ray spectroscopy (SEM/EDX), hard X-ray photoelectron spectroscopy (HAXPES), and in situ grazing incidence X-ray diffraction (GI-XRD) to investigate phase transformations of the film under near-reduction conditions. Synchrotron-based methods were applied due to the ultralow thickness of the catalyst film and to probe the functional interface between the active metal and support. The catalytic properties were determined in a fixed-bed reactor at various total flow rates.

MATERIALS AND METHODS

The sample is prepared by deposition of a 100 nm layer of SiO_x by PECVD using silane (SiH_4) and nitrous oxide (N_2O) as precursor gas onto a 10 cm × 10 cm aluminum foil (Thermo scientific, Puratronic 0.1 mm (0.004 in) thick, Purity: 99.997% (metal basis)) substrate, resulting in a SiO_x/Al substrate stack. The SiO_x/Al stack is followed by a 25 nm layer deposition of cobalt by using magnetron sputtering, resulting in a Co-SiO_x/Al thin-film catalyst stack. The deposited SiO_x acts as a buffer interlayer, stabilizing the cobalt layer and preventing it from reacting with Al (i.e., alloy formation). Afterward, the resulting thin-film catalyst was calcined in a static oven at 350 °C overnight to obtain a *spinel*-Co_3O_4 layer. The morphology and thickness of the synthesized thin film catalyst were then investigated using a scanning electron microscope (SEM) LEO GEMINI 1530 instrument from ZEISS at an acceleration voltage of 15 kV. A first estimate of

https://doi.org/10.1021/acs.iecr.5c02728
Ind. Eng. Chem. Res. 2025, 64, 22939−22948

the composition of the thin film was obtained by energy dispersive X-ray spectroscopy (EDX) at prepared cross sections.

Catalyst Testing. A total of 0.166 g (2.75 cm × 2 cm) of Co-SiO_x/Al thin film catalyst was cut into small pieces, mixed with SiC (300 mesh), and loaded into a fixed-bed reactor, see Supporting Information Figure S1 for the reactor schematic. Prior to FTS testing, the loaded catalyst was reduced in situ in flowing H_2 at 200 mL(NTP)/min for 16 h at 350 °C. The FTS catalytic activity of the Co-SiO_x/Al thin film catalyst was then tested at 220 °C, 20 bar, and various total gas flow rates of 40 mL/min, 20 mL/min, and 5 mL/min using a syngas premix (60% H_2−30% CO in Ar) with a H_2/CO ratio of 2.

Material Characterization. The chemical and electronic properties at and near the surface of the as-synthesized Co-SiO_x/Al thin film catalyst were investigated via HAXPES at the HiKE endstation located at BESSY II's KMC-1 beamline operated by HZB.[12] The endstation has a base pressure <1 × 10^{-8} mbar and is equipped with a Scienta R4000 electron analyzer, enabling utilization of the excitation energy range (2−10 keV) provided by the KMC-1 bending magnet beamline. For this work, two different excitation energies were employed, 2.5 and 4.0 keV, using the Si(111) and Si(311) crystal pairs of the KMC-1 double crystal monochromator, respectively. For energy scale calibration, Au 4f spectra were measured from a clean gold film, setting the peak position of Au $4f_{7/2}$ to be at a binding energy (BE) of 84.00 eV; any deviation from this value was used to shift all recorded spectra accordingly.

The crystallographic phase of the cobalt moiety (i.e., *hcp*- or *fcc*-Co^0) can determine the overall intrinsic activity during FTS, with *hcp*-Co^0 showing higher activity compared to *fcc*-Co^0.[13,14] Thus, optimization of the crystallographic phase of the thin-film catalyst is essential, as it can impact the overall performance of the catalyst. As such, the phase transformation of *spinel*-Co_3O_4 over a temperature range up to 350 °C under reduction conditions was investigated using the in situ synchrotron grazing incident XRD (GI-XRD) technique. Since this characterization technique necessitates a flat substrate, instead of using aluminum foil, fused silica wafers (MicroChemicals, JGS1 wafer 2 in.; 500 ± 25 μm, 2-sided polished, TTV <10 μm, 1 SEMI Flat) were used as substrates to deposit a 25 nm cobalt layer by magnetron sputtering. The in situ synchrotron GI-XRD was conducted at beamline KMC-2 at BESSY II operated by HZB. The spectral characteristics of KMC-2 offer high-photon flux within 8−10 keV, which, combined with the 2D Bruker Vantec 2000 detector (using Cu-Kα radiation), provides sufficient time resolution and surface sensitivity using low incident angles (ω = 2°). This is important for the investigation of the phase change of cobalt under reduction conditions at elevated temperatures. KMC-2/Diffraction is equipped with an X-ray transparent furnace (Anton Paar DHS 1100) that is suitable for performing high-temperature in situ synchrotron GI-XRD studies under a reducing atmosphere.

RESULTS AND DISCUSSION

The surface morphology of the as-synthesized Co-SiO_x/Al thin-film catalyst was analyzed by using SEM to assess whether the thin film forms a continuous, closed layer. An overview of the surface morphology of the synthesized Co-SiO_x/Al thin-film catalyst is depicted in Figure 1a. Moreover, Figure 1b presents a high-resolution SEM image depicting the surface morphology of the as-synthesized Co-SiO_x/Al thin-film catalyst. Evidently, in Figure 1a,b, there are no obvious morphological defects in the as-synthesized thin film catalyst, suggesting a continuous film without an open film structure or island formation. SEM−EDX analysis was used as a preliminary screening method to determine the elemental composition of the overall thin-film catalyst, as shown in Supporting Information Figure S2. However, this technique has limitations for thin-film characterization due to its significant penetration depth, which can lead to contributions from the underlying aluminum substrate, thus reducing the accuracy of the compositional analysis. However, the overall thin-film catalyst composition can be determined, expectedly with Al, Co, and Si as the main elements in the thin-film catalyst. A more detailed chemical composition of the thin-film catalyst sample by HAXPES is discussed below. Furthermore, the total thickness of the deposited Co and SiO_x layer was confirmed by cross-sectional SEM analysis, as shown in Figure 1c. A total thickness of approximately 120 nm was determined. The measured total thickness is slightly lower than the targeted total thickness of 125 nm (with the SiO_x layer contributing *ca.* 100 nm, while the cobalt layer accounts for approximately 25 nm). This deviation may stem from poor contrast between the different layers at the thin-film interface, along with the inherent unevenness of the aluminum foil substrate, which may lead to an underestimation of the total layer thickness. The overall thin-film layer elemental cross-section mapping of the measured 120 nm thickness was determined, as shown in Figure 1d. The Si signal becomes more pronounced halfway through the analysis line (shown in Figure 1d) and then decreases drastically, while the Co signal increases (coinciding with a drastic decrease in the Si signal) at the edge of the thin-film catalyst sample. This observation may indicate that the SiO_x buffering layer and the Co layer exist as distinct, separate layers rather than forming a uniform gradient or intermixing layers. Nevertheless, further speciation of the cobalt layer will be determined using a more surface-sensitive technique to determine a possible alloy formation, as reported below.

The chemical and electronic properties at and near the surface of the as-synthesized Co-SiO_x/Al thin-film catalyst (before any gas treatment) were investigated via HAXPES using 2.5 and 4.0 keV excitation. This approach enables depth-resolved analysis of the chemical composition of the thin-film layer. The increased inelastic mean free path (IMFP) of the emitted electrons with high kinetic energy facilitates investigations of chemical properties and electronic states in the bulk of materials and at buried interfaces. Analysis conducted at 2.5 keV excitation energy provides insights into the chemical structure of the first approximately 5−10 nm of the thin film, while analysis at 4.0 keV excitation energy extends the analysis to a depth of ca. 10−15 nm, as illustrated in Supporting Information Figure S3. It is important to note that these penetration depths are expressed as ranges, as the signal detected for HAXPES core levels is effectively integrated over a volume defined by an exponential function. This exponential function depends on the inelastic mean free path (IMFP) of the investigated photoelectrons through the investigated sample. As a rule, the photoemission signal will be dominated by the region closer to the surface (i.e., ∼63% of the signal will originate from the region equivalent to the topmost IMFP value). In the case of metal Co, photoelectrons with kinetic energies (KE) of 2.5 and 4.0 keV (i.e., the maximum attainable KE values with 2.5 and 4.0 keV excitation,

https://doi.org/10.1021/acs.iecr.5c02728
Ind. Eng. Chem. Res. 2025, 64, 22939−22948

respectively) will exhibit IMFP values of 3.1 and 4.6 nm, respectively.[15]

First, survey spectra of the Co-SiO_x/Al thin film catalyst were obtained at 2.5 and 4.0 keV, as shown in Figure 2a. At

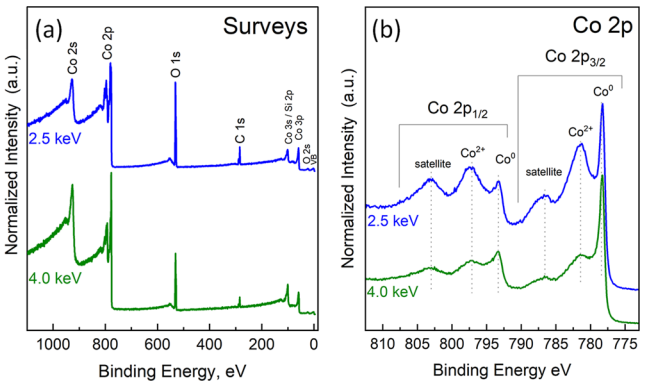

Figure 2. (a) HAXPES survey and (b) detailed spectra of the Co 2p energy region of the Co-SiO_x/Al thin-film catalyst measured using 2.5 and 4.0 keV excitation energy.

both excitation energies, as expected, the survey spectra for Co-SiO_x/Al thin film confirmed the presence of Co- and O-related core levels associated with cobalt oxide species present in the thin film. Moreover, a carbon peak associated with adventitious carbon is also detected.

Figure 2b shows HAXPES detail spectra of the Co 2p energy region, as measured using 2.5 and 4.0 keV. Peaks assigned to Co $2p_{3/2}$ and Co $2p_{1/2}$ lines for different Co chemical environment contributions can be observed: multiple peaks with binding energies centered at 778.42 eV (Co $2p_{3/2}$) and 793.22 eV (Co $2p_{1/2}$), corresponding to metallic cobalt (Co^0) and at 781.52 eV (Co $2p_{3/2}$) and 797.42 eV (Co $2p_{1/2}$), attributed to divalent (Co^{2+}) cobalt(II) oxide, with also a possibility of $Co(OH)_2$ species.[16] Additionally, two satellite peaks with binding energies of 786.82 eV (Co $2p_{3/2}$) and 803.22 eV (Co $2p_{3/2}$) were identified, related to the multiplet splitting pattern of the Co oxide contribution.[17] Further chemical composition analysis of the approximately 10−15 nm depth of the thin film layer was conducted by increasing the excitation energy to 4.0 keV. Similar to the spectrum obtained at a 2.5 keV excitation energy, the two peaks at the Co 2p energy level are ascribed to Co $2p_{3/2}$ and Co $2p_{1/2}$, respectively. Each peak shows signal contribution related to various chemical states, with binding energies centered at 778.42 eV (Co $2p_{3/2}$) and 793.22 eV (Co $2p_{1/2}$), corresponding to elemental cobalt (Co^0), and at 781.52 eV (Co $2p_{3/2}$) and 797.42 eV (Co $2p_{1/2}$), attributed to divalent (Co^{2+}) cobalt(II) oxide. Likewise, two satellite peaks with binding energies of 786.82 eV (Co $2p_{3/2}$) and 803.22 eV (Co $2p_{1/2}$) were identified.

The metallic cobalt contribution is observed to be clearly more pronounced in the 4.0 keV excited spectrum (i.e., in the measurement with greater probing depth) compared to the 2.5 keV excited spectrum (i.e., which represents the more surface-sensitive measurement). Based on this, it can be inferred that the cobalt moiety in the bulk of the thin-film catalyst predominantly exists as metallic cobalt (e.g., as initially deposited), while cobalt(II) oxide species are detected (due to the presence of nominal oxidation state Co^{2+}) at the surface of the sample, likely forming upon exposure to the atmospheric environment during storage. Thus, the observed cobalt oxide species is ascribed to an unavoidable vacuum break during sample transfer from the sputter system to the KMC-2 beamline station. Although undesired, we note that this surface oxidation is of little consequence to subsequent catalytic activity, as the sample is fully calcined to *spinel*-Co_3O_4 before use for FTS, as discussed later.

Noteworthy, peaks indicative of alloy formation between the cobalt layer and the buffering layer (SiO_2), such as cobalt silicate species, were not observed. This may indicate that the interface between the SiO_x and Co layers does not exist as an alloy.

The coexistence of the metallic cobalt and cobalt oxide phases poses a challenge in accurately quantifying the degree of reduction of the cobalt layer during the reduction step before FTS. To address this, the sample was first fully oxidized to the most stable phase, i.e., *spinel*-Co_3O_4, followed by a reduction step to activate the catalyst for FTS. Accordingly, the as-prepared Co-SiO_x/Al thin-film catalyst was fully oxidized in an oxygen atmosphere to obtain a *spinel*-Co_3O_4 layer of the Co-SiO_x/Al thin-film catalyst. Thus, before FTS catalyst testing, the thin-film catalyst is reduced to metallic cobalt, which is the active phase for FTS. This reduction step becomes crucial during FTS, as it may determine the crystallographic phase that forms during the formation of metallic cobalt. As aforementioned, *hcp*-Co^0 exhibits better catalytic FTS activity compared to the *fcc*-Co^0 phase.[13,18] Thus, optimizing the reduction step such that the formation of the *hcp*-Co^0 phase is more favored becomes essential. Thus, in situ synchrotron GI-XRD analysis was employed to determine the crystallographic transformation of the Co layer of the thin film during reduction. This characterization technique necessitates a relatively flat and smooth surface to ensure uniform grazing incidence of X-rays, as excessive roughness can lead to scattering and a reduced diffraction signal. Due to the inherent uneven surface of the regularly used aluminum foil substrate used for the Co-SiO_x/Al catalyst, a SiO_2 wafer was used as the substrate instead to probe the crystallographic change of the cobalt layer during reduction using in situ synchrotron GI-XRD. The surface morphology of the as-synthesized Co/SiO_2 sample is shown in Figure 3a. The sample was then oxidized at 350 °C, and the surface morphology of the oxidized Co/SiO_2 sample is shown

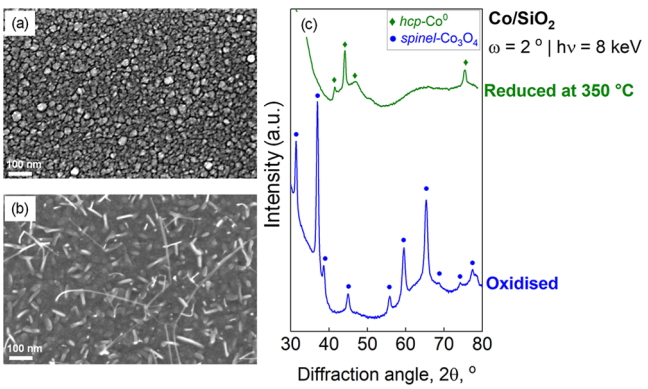

Figure 3. Surface morphology of the (a) as-synthesized and (b) oxidized Co/SiO_2 model catalyst used for the in situ synchrotron GI-XRD experiment, (c) in situ synchrotron GI-XRD pattern of the Co/SiO_2 thin-film model catalyst at 30 °C and at 350 °C in reduction conditions.

https://doi.org/10.1021/acs.iecr.5c02728
Ind. Eng. Chem. Res. 2025, 64, 22939−22948

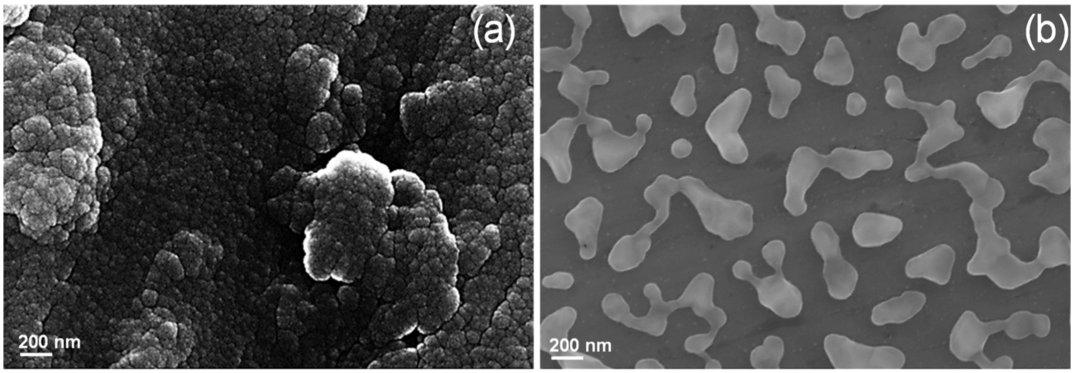

Figure 4. SEM images of Co-SiO_x/Al thin film catalyst (a) as-synthesized and (b) after calcination and reduction treatment at 350 °C.

in Figure 3b. Evidently, no sample dewetting is observed upon oxidation of the sample at 350 °C.

First, the crystallographic structure of the oxidized Co/SiO_2 catalyst sample was examined with grazing incidence X-ray diffraction. The resulting in situ synchrotron GI-XRD pattern, presented in Figure 3c, shows distinctive peaks which correspond to the (220), (311), (222), (400), (422), (511), (440), (620), and (533) planes and represent the characteristic diffraction pattern of *spinel*-Co_3O_4. Subsequently, the sample was heated from 35 to 350 °C in a reductive environment, and the crystallographic morphology of the samples was re-examined with in situ synchrotron GI-XRD at 350 °C. Diffraction peaks at 2θ = 41.6°, 44.2°, 47.2°, and 75.6° corresponding to the (100), (002), (101), and (110) crystallographic planes, respectively, were observed. This suggests that under reduction conditions at 350 °C under flowing H_2, the cobalt moiety of the sample exists as hexagonal-closed-packed metallic cobalt, *hcp*-Co^0.

No diffraction peaks corresponding to the *fcc*-Co^0 and cobalt(II)oxide phases were observed. Hence, these conditions are considered sufficient to activate the Co-SiO_x/Al thin-film catalyst for the FTS process later in this contribution.

Notably, it can be argued that the cobalt moiety interacts differently between the Co/SiO_2 thin-film catalyst on fused silica and the Co-SiO_x/Al thin-film catalyst. However, the interaction between Co and SiO_2 of the Co/SiO_2 model catalyst and between Co and SiO_x of the Co-SiO_x/Al thin-film catalyst is assumed to be comparable.

The morphological changes associated with the oxidation-followed-by-reduction treatment at 350 °C on the Co/SiO_2 sample could not be examined by SEM−EDX due to sample charging. Thus, the working catalyst, Co-SiO_x/Al thin film, was oxidized followed by reduction at 350 °C, similar to the Co/SiO_2 model catalyst, mimicking the sample preparation before FTS operation. However, this thin-film catalyst gas and thermal treatment may result in a thin-film structural reconstruction, which may ultimately alter the morphology of the film. The morphological structure of the Co-SiO_x/Al thin film postoxidation and reduction treatment was examined under SEM Figure 4a depicts the catalyst surface morphology of the Co-SiO_x/Al thin film before calcination and reduction, while Figure 4b shows the catalyst surface morphology after treatment. Evidently, before gas and thermal treatment, the thin film is closed and continuous, after which, upon gas and thermal treatment, a layer reconstruction with island formation is observed. This phenomenon of dewetting in thin-film-deposited catalysts upon thermal and gaseous treatment has been previously reported.[19] The observed reconstruction of the deposited thin-film catalyst is analogous to particle sintering in powder catalyst systems and is well-known in literature for nonreactive wetting at inert interfaces.

In cobalt-based powder catalyst systems, the addition of structural promoters such as Mn to inhibit particle sintering is a common practice;[20,21] a similar approach can be considered for thin-film catalysts. However, varying the buffering layer of the thin-film catalyst can also inhibit surface reconstruction of the deposited layer during gas and thermal treatment.[22] A study is currently underway to investigate the effect of different buffer interlayers on the morphological stability of cobalt-based thin films under gas exposure and thermal treatment. Understanding how various buffer materials influence the structural integrity and catalytic performance of the thin film under FTS operating conditions is beyond the scope of this study and will be published at a later stage.

Fischer−Tropsch Synthesis Catalyst Testing. Our Co-SiO_x/Al thin-film catalyst, with 0.07 wt % Co loading, was evaluated for FTS activity at various total gas flow rates of 40, 20, and 5 sccm. At 40 sccm total gas flow rate, a CO conversion of 0.9% was obtained. Upon decreasing the total gas flow rate from 40 to 20 sccm, the CO conversion slightly increased to 1.2%. Further decreasing the total flow rate to 5 mL/min yielded a CO conversion of 2.7%, as shown in Figure 5a.

The increase in CO conversion levels with decreasing total gas flow rate is expected, as a decreased flow rate increases the residence time of the reactive gas on the catalyst bed, allowing more time for the reaction to occur. However, theoretically, a decrease in flow rate is expected to inversely increase the

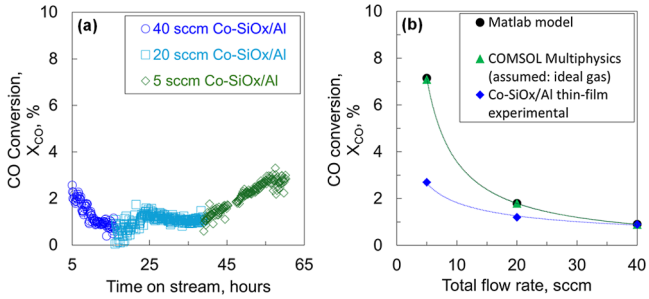

Figure 5. (a) Time-dependent CO conversion levels for the Co-SiO_x/Al thin film catalyst at varying total flow rates, illustrating the effect of flow rate on X_{CO} levels. (b) Comparison of experimentally obtained CO conversion levels at various total flow rates with simulated trends, including models with and without the boundary layer effect.

https://doi.org/10.1021/acs.iecr.5c02728
Ind. Eng. Chem. Res. 2025, 64, 22939−22948

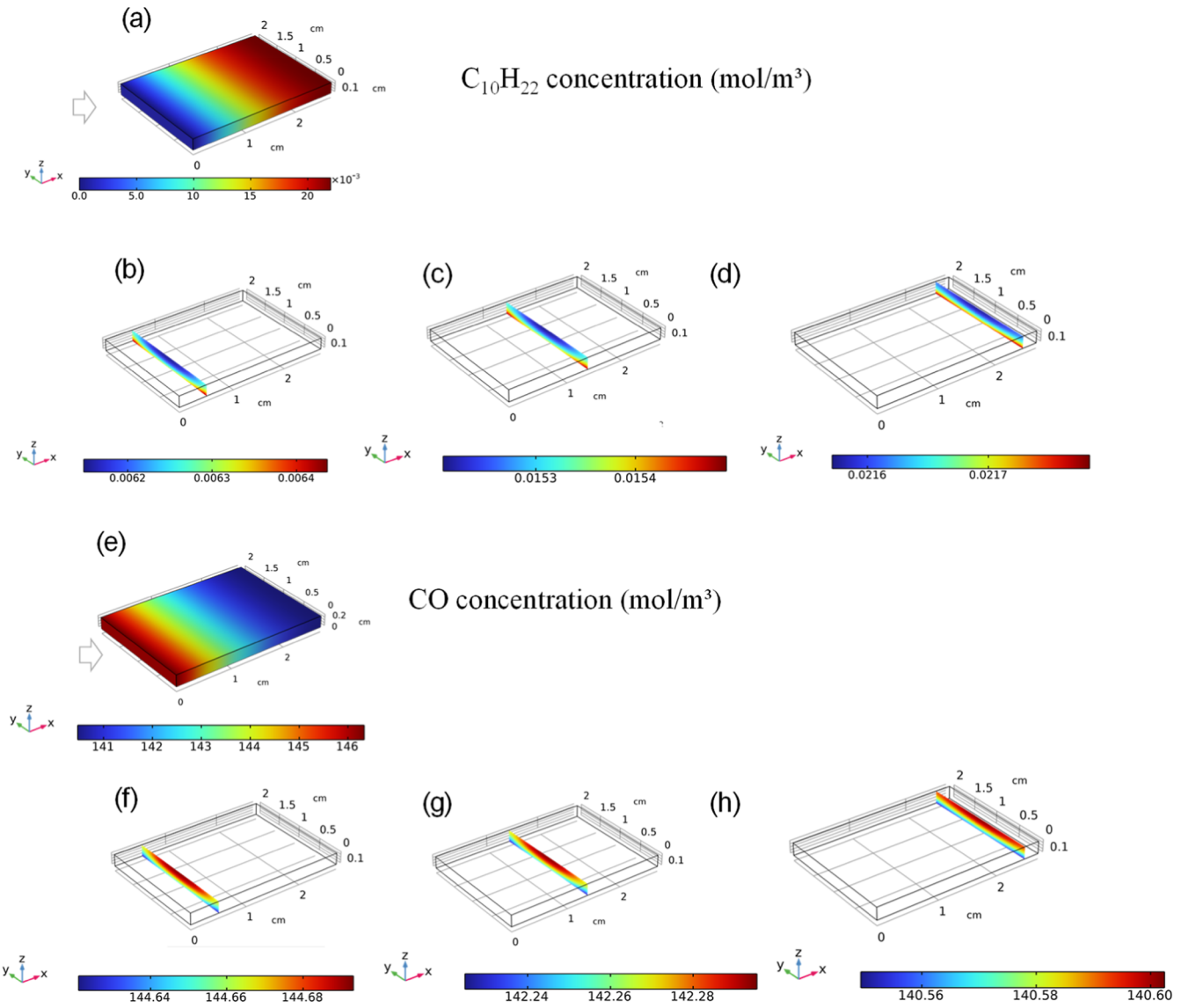

Figure 6. Multiphysics modeling for 3-D reactor channel at 5 sccm. Concentration profile at the inlet (b,f), middle (c g), and outlet (d,h) of the multichannel reactor for $C_{10}H_{22}$ (a−d) and CO (e−h).

conversion level, as the residence time increases with decreasing flow rate. Gavrilović et al. also observed an increase in CO conversion with a proportional decrease in syngas flow rate.[23] In the present study, when the total flow rate was decreased from 40 to 20 sccm, the CO conversion was expected to increase from 0.9% to 1.8%. However, only a CO conversion of 1.2% was achieved at 20 sccm. This trend of lower-than-expected CO conversion became more pronounced with a further decrease in the total flow rate to 5 sccm. Specifically, decreasing the flow rate from 40 to 5 sccm was expected to yield a CO conversion of approximately 7.2% when considering the 0.9% CO conversion level obtained at 40 sccm; instead, only 2.7% was observed.

The experimentally lower-than-expected CO conversion at total flow rates of 20 and 5 sccm may indicate severe external mass transfer limitations. This may be due to low velocity profiles, where pronounced boundary layers are formed and become more distinct with decreasing flow rate. The reactants from the bulk flow are mainly transported via diffusion through stagnant or very slow fluid layers to the catalyst surface. Similarly, the diffusion of the formed products back to the bulk flow is slowed, which can subsequently restrict access to the catalyst surface not only by boundary layers but also by pronounced product layers (for example, long-chain liquid hydrocarbons formed during FTS). As a subsequent external mass transfer, limitations may be observed.

To gain insights into these potential limitations, kinetic simulations with different model (MATLAB model and COMSOL Multiphysics) assumptions were employed. The details of this approach will be published elsewhere soon. CO conversion levels in an ideal plug flow reactor (without boundary layer effects)—MATLAB Model—and a microchannel reactor from COMSOL Multiphysics simulations, assuming ideal-gas phases and isothermal conditions (a model that would detect the effects of the boundary layers due to the laminar flow pattern), are compared in Figure 5b. It is also important to note that the hydrodynamic properties in the microchannel reactor (used for the COMSOL Multiphysics simulation) differ significantly from those in the fixed bed used in the experimental investigation previously reported herein. The fixed bed tends to have relatively thinner boundary layers due to its random packing. On the other hand, the

https://doi.org/10.1021/acs.iecr.5c02728
Ind. Eng. Chem. Res. 2025, 64, 22939−22948

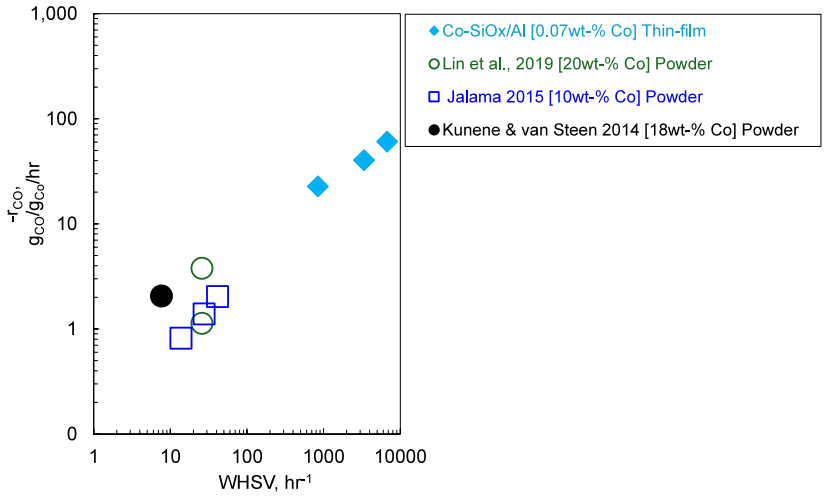

Figure 7. Rate of CO consumption ($-r_{CO}$) comparison between the thin-film Co-SiO_x/Al catalyst and classical powder cobalt-based catalysts.

microchannel exhibits typical laminar flow, enhancing the effect of the boundary layer. As such, the simulations mainly evaluate the maximum potential impact of boundary layers posed by the flow pattern at various total gas flow rates on external mass transfer limitations.

Thus, the simulation results indicate that the boundary layers have a negligible effect on CO conversion at flow rates of 20 and 5 sccm, as shown in Figure 5b. However, the measured activity observed over the Co-SiO_x/Al thin film catalyst is lower even after considering boundary layer effects. This suggests that the lower-than-expected CO conversion obtained over the Co-SiO_x/Al thin-film catalyst cannot be solely attributed to external mass transfer limitations associated with boundary layer effects.

Therefore, it is proposed that the formation of C_{5+} liquid products may also contribute to the limitations in external mass transfer limitations. Figure 6 illustrates the concentration profiles of $C_{10}H_{22}$, as a model long-chain FTS product (shown in Figure 6a) and CO (depicted in Figure 6e) at the inlet (cf. Figure 6b,f), middle (cf. Figure 6c,g), and outlet (cf. Figure 6d,h) of the microchannel reactor (MCR). Due to the pronounced external mass transfer limitations observed under low flow rates in the experiment, 5 sccm was specifically chosen for the simulation. Figure 6a highlights that the $C_{10}H_{22}$ concentration increases from the inlet to the outlet across the MCR; inversely, the CO concentration at the surface of the thin-film catalyst decreases across the MCR, as shown in Figure 6e. Notably, the increase in the level of $C_{10}H_{22}$ product formation coincides with a decrease in the CO concentration closer to the catalyst surface across the reactor. This suggests that CO easily accesses most of the catalyst surface, except for the corners, while near the outlet, the overall access of CO to the catalyst surface is limited. Thus, it can be inferred that the formation of the $C_{10}H_{22}$ product on the thin-film catalyst may impede the diffusion of CO to the active sites, ultimately decreasing the intrinsic catalytic activity of the thin-film catalyst.

Despite the hypothesized severe external mass transfer limitation, considering the cobalt metal loading of 0.07 wt %Co in the sample tested, the rate of CO consumption ($-r_{CO}$) was *ca.* 23, 40, and 61 $g_{CO}/g_{Co}/h$ for weighted hourly space velocity (WHSV) of 840, 3370, and 6736 h^{-1}, respectively, as shown in Figure 7. Typically, for a powder cobalt-based catalyst, the rate of CO consumption for the unpromoted catalyst is approximately 68 $g_{CO}/g_{Co}/h$.[24] A comparison of $-r_{CO}$ obtained from the tested thin-film catalyst with classical powder catalyst systems suggests that the Co-SiO_x/Al thin-film catalyst demonstrates a higher $-r_{CO}$ than a typical unpromoted powder system.[25−27] Therefore, the relatively low CO conversion observed over the Co-SiO_x/Al thin film may be attributed to a low cobalt metal loading rather than an intrinsically low catalytic activity of the sample. Though caution must be exercised, as differences in parameters such as surface accessibility and pore diffusion between the powder and thin-film catalysts can lead to variations in the mass transfer coefficient, which may ultimately result in discrepancies in the observed catalytic activity.

Despite the reported higher $-r_{CO}$ obtained over the thin-film catalyst in relation to the powder catalyst, it should be noted that the volumetric productivity of the fixed-bed reactor may influence and pose an underestimation of the intrinsic catalytic activity, particularly for the thin-film catalyst. Microchannel reactors, with their significantly higher volumetric productivity, are better suited to thin-film catalysis. Nevertheless, a meaningful comparison between thin-film and powder catalysts requires the use of a reactor capable of accommodating both to minimize external variables that directly influence their performance. As such, this study considered a fixed-bed reactor for comparison. However, in the subsequent stages of this study, beyond the comparative assessment of the catalytic performance between thin-film and powder catalyst systems, an appropriate microchannel reactor (MCR) will be employed to precisely quantify the performance of the thin-film catalyst systems.

Product Selectivity Profile Consideration. The product selectivity profile obtained over the Co-SiO_x/Al thin-film catalyst at total gas flow rates of 40, 20, and 5 sccm was evaluated. Methane selectivity of 72, 56, and 48% at 0.9, 1.2, and 2.7% CO conversion levels was obtained at 40, 20, and 5 sccm flow rates, respectively. Ma et al. showed that methane selectivity is affected by the catalytic CO conversion levels, especially at relatively lower and higher CO conversions.[28,29] The methane selectivity is related to the probability of surface carbon being hydrogenated to a surface methyl species and subsequently hydrogenated to methane.[30] This makes methane selectivity a rather complex variable; the increase in the CH_4-

https://doi.org/10.1021/acs.iecr.5c02728
Ind. Eng. Chem. Res. 2025, 64, 22939−22948

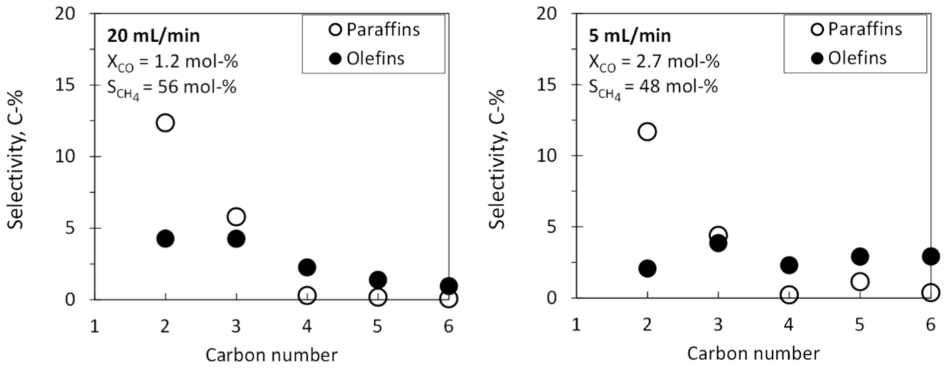

Figure 8. Comparison of paraffin and olefin distribution over the Co-SiO_x/Al thin-film catalyst at a total gas flow rate of 20 and 5 sccm.

selectivity with increasing conversion may be related to the lack of monomeric species for chain growth in close proximity to the growing chain at low conversion as a consequence of the high coverage of the surface with CO and carbon.[30] In the current study, overall low CO conversion levels are reported, and in accordance with the findings of Ma et al.[28,29] a significant decrease in CH_4 selectivity is observed with an increase in CO conversion levels upon decreasing the gas flow rate from 40 to 5 sccm. This may suggest that the observed CH_4 selectivity is strongly influenced by CO conversion levels obtained over 0.07 wt %Co-SiO_x/Al thin-film catalyst. Moreover, by virtue of low CO conversion levels, the C−C coupling rate is diminished due to a low concentration of dissociated CO on the surface, resulting in a low coverage of monomeric species. This subsequently reduces the C_{5+} selectivity, hence the observed relatively high CH_4 selectivity. The chain growth probability, α_1, was determined to be 0.44, 0.37, and 0.48, corresponding to 40, 20, and 5 sccm, respectively. This further signifies a limited C−C coupling rate, which may result in high C_{5+} selectivity.

The α−olefin selectivity was determined in comparison to that of the formed paraffins. Olefin content selectivity may indicate hydrogenation of the surface species during the FTS process. In relation to paraffins, α-olefin content in the fraction of linear hydrocarbons was observed to be higher than that of paraffins at comparable carbon number, except for C_2, as shown in Figure 8. The olefin/paraffin (O/P) ratio for the vapor phase (C_3−C_7 range) was determined to be 2.21, 1.41, and 1.96, corresponding to the total gas flow rate of 40, 20, and 5 sccm, respectively. This further indicates that the hydrogenation rate of the surface species to form paraffin hydrocarbons may not be the dominant factor.

The C_2 olefin fraction is typically observed to be lower compared to the C_3 content in the Anderson−Schulz−Flory (ASF) plot. This is attributed to re-adsorption of ethylene for secondary reactions, thus decreasing its concentration. The ASF plot from the C_1−C_7 carbon range of the total is reported in Figure S4 of the Supporting Information. Due to the low yields of the oil and aqueous phase (2 g of total liquid recovered at steady-state), a full ASF plot and α_2 could not be determined.

CONCLUSION

This work serves as a proof of concept, demonstrating the applicability of cobalt-based thin-film catalysts in the Fischer−Tropsch synthesis process. A Co-SiO_x/Al thin-film catalyst was synthesized using plasma-enhanced chemical vapor deposition (PECVD) and magnetron sputtering, with a cobalt metal loading of 0.07 wt %. HAXPES characterization results support the idea that the cobalt layer in the as-synthesized catalyst was deposited as metallic cobalt, with no evidence of alloy formation between the SiO_x buffer interlayer and the cobalt layer. Under reductive conditions at 350 °C, the *hcp*-Co^0 phase, which is the preferred crystallographic structure for FTS, was obtained from the *spinel*-Co_3O_4 moiety of the catalyst.

Despite severe mass transfer limitations, the thin-film catalyst system exhibited a performance that matches or even surpasses that of traditional powder-based catalyst systems in terms of rate of CO consumption ($-r_{CO}$). This positions thin-film catalysts as a viable alternative in FTS, offering advantages such as enhanced catalytic efficiency, potential cost reduction, and improved control over catalyst structure and performance. Additionally, thin-film catalysts could contribute to process intensification, promoting effective catalyst design, improved characterization methods, and scalability for high-grade hydrocarbon production.

While the thin-film catalyst exhibits a performance that might be equal to or even surpass conventional catalysts, future optimizations are necessary to improve catalyst stability and longevity. In addition, the observed performance of the thin-film catalyst in a fixed-bed reactor motivates catalyst testing of the thin-film catalyst in a microchannel reactor, which is compatible with this type of catalyst but also has significantly higher volumetric productivity.

ASSOCIATED CONTENT

Supporting Information

The Supporting Information is available free of charge at https://pubs.acs.org/doi/10.1021/acs.iecr.5c02728.

Reactor packing schematic, SEM−EDX elemental composition of the Co-SiO_x/Al thin-film catalyst, schematic representation of the penetration depths associated with the 2.5 and 4.0 keV excitation energies of HAXPES, and ASF distribution plot with different α values of various total gas flow rates over Co-SiO_x/Al thin-film catalysts (PDF)

AUTHOR INFORMATION

Corresponding Author

Avela Kunene − *Helmholtz-Zentrum Berlin für Materialien und Energie GmbH (HZB), Berlin 141901, Germany;* orcid.org/0000-0001-9417-9870; Email: avela.kunene@helmholtz-berlin.de

https://doi.org/10.1021/acs.iecr.5c02728
Ind. Eng. Chem. Res. 2025, 64, 22939−22948

Authors

Yangjun Wei − *Helmholtz-Zentrum Berlin für Materialien und Energie GmbH (HZB), Berlin 141901, Germany*

Eric van Steen − *Catalysis Institute, University of Cape Town, Rondebosch, Cape Town 7701, South Africa;* orcid.org/0000-0003-4659-8522

Muhammad Hamid Raza − *Helmholtz-Zentrum Berlin für Materialien und Energie GmbH (HZB), Berlin 141901, Germany;* orcid.org/0000-0003-0061-5139

Imane El Arrouji − *Helmholtz-Zentrum Berlin für Materialien und Energie GmbH (HZB), Berlin 141901, Germany*

Catalina E. Jimenez − *Helmholtz-Zentrum Berlin für Materialien und Energie GmbH (HZB), Berlin 141901, Germany;* orcid.org/0000-0002-8107-4399

Roberto Félix − *Helmholtz-Zentrum Berlin für Materialien und Energie GmbH (HZB), Berlin 141901, Germany;* orcid.org/0000-0002-3620-9899

Daniel M. Toebbens − *Helmholtz-Zentrum Berlin für Materialien und Energie GmbH (HZB), Berlin 141901, Germany*

Ali Shan Malik − *Helmholtz-Zentrum Berlin für Materialien und Energie GmbH (HZB), Berlin 141901, Germany*

Veroushia Padayachee − *Catalysis Institute, University of Cape Town, Rondebosch, Cape Town 7701, South Africa*

Dominic De Oliveira − *Catalysis Institute, University of Cape Town, Rondebosch, Cape Town 7701, South Africa*

Mohamed Islam Fadlalla − *Catalysis Institute, University of Cape Town, Rondebosch, Cape Town 7701, South Africa*

Marcus Bär − *Helmholtz-Zentrum Berlin für Materialien und Energie GmbH (HZB), Berlin 141901, Germany; Friedrich-Alexander Universität Erlangen-Nürnberg (FAU), Erlangen 91058, Germany; Helmholtz Institute Erlangen-Nürnberg for Renewable Energy (HI ERN), Berlin 12489, Germany;* orcid.org/0000-0001-8581-0691

Sonya Calnan − *Helmholtz-Zentrum Berlin für Materialien und Energie GmbH (HZB), Berlin 141901, Germany;* Present Address: Loughborough University, Loughborough, Leicestershire, LE11 3TU (United Kingdom)

Michael Claeys − *Catalysis Institute, University of Cape Town, Rondebosch, Cape Town 7701, South Africa;* orcid.org/0000-0002-5797-5023

Rutger Schlatmann − *Helmholtz-Zentrum Berlin für Materialien und Energie GmbH (HZB), Berlin 141901, Germany;* orcid.org/0000-0002-5951-9435

Daniel Amkreutz − *Helmholtz-Zentrum Berlin für Materialien und Energie GmbH (HZB), Berlin 141901, Germany*

Complete contact information is available at: https://pubs.acs.org/10.1021/acs.iecr.5c02728

Notes

The authors declare no competing financial interest.

■ ACKNOWLEDGMENTS

The authors gratefully acknowledge the financial support of the German Federal Ministry of Education and Research (BMBF) within the CARE-O-SENE project (03SF0673). The authors thank Helmholtz-Zentrum Berlin für Materialien und Energie GmbH for the allocation of synchrotron radiation beamtime. Special gratitude is extended to Alex Steigert and Tobias Köhler for their assistance with sample preparation and to Florian Ruske for his expertise in SEM imaging.

■ REFERENCES

(1) Kubička, D.; Černý, R. Upgrading of Fischer−Tropsch Waxes by Fluid Catalytic Cracking. *Ind. Eng. Chem. Res.* **2012**, *51*, 8849−8857.

(2) Neuner, P.; Graf, D.; Mild, H.; Rauch, R. Catalytic Hydroisomerisation of Fischer−Tropsch Waxes to Lubricating Oil and Investigation of the Correlation between Its Physical Properties and the Chemical Composition of the Corresponding Fuel Fractions. *Energies* **2021**, *14* (14), 4202−4216.

(3) Khodakov, A. Y.; Chu, W.; Fongarland, P. Advances in the Development of Novel Cobalt Fischer−Tropsch Catalysts for Synthesis of Long-Chain Hydrocarbons and Clean Fuels. *Chem. Rev.* **2007**, *107* (5), 1692−1744.

(4) Apolinar-Hernández, J.; Bertoli, S.; Riella, H.; Soares, C.; Padoin, N. An Overview of Low-Temperature Fischer−Tropsch Synthesis: Market Conditions, Raw Materials, Reactors, Scale-Up, Process Intensification, Mechanisms, and Outlook. *Energy Fuels* **2024**, *38*, 1−28.

(5) Tsakoumis, N. E.; Rønning, M.; Borg, Ø.; Rytter, E.; Holmen, A. Deactivation of Cobalt Based Fischer−Tropsch Catalysts: A Review. *Catal. Today* **2010**, *154* (3), 162−182.

(6) Claeys, M.; Dry, M. E.; van Steen, E.; du Plessis, E.; van Berge, P. J.; Saib, A. M.; Moodley, D. J. In Situ Magnetometer Study on the Formation and Stability of Cobalt Carbide in Fischer−Tropsch Synthesis. *J. Catal.* **2014**, *318*, 193−202.

(7) Post, M. F. M.; Van't Hoog, A. C.; Minderhoud, J. K.; Sie, S. T. Diffusion Limitations in Fischer−Tropsch Catalysts. *AIChE J.* **1989**, *35* (7), 1107−1114.

(8) Duerksen, A.; Thiessen, J.; Kern, C.; Jess, A. Fischer−Tropsch Synthesis with Periodical Draining of a Liquid-Filled Catalyst by Hydrogenolysis. *Sustain. Energy Fuels* **2020**, *4* (4), 2055−2064.

(9) Xu, B.; Fan, Y.; Zhang, Y.; Tsubaki, N. Pore Diffusion Simulation Model of Bimodal Catalyst for Fischer−Tropsch Synthesis. *AIChE J.* **2005**, *51* (7), 2068−2076.

(10) Trinh, C.; Wei, Y.; Yadav, A.; Muske, M.; Grimm, N.; Li, Z.; Thum, L.; Wallacher, D.; Schlögl, R.; Skorupska, K.; Schlatmann, R.; Amkreutz, D. Reactor Design for Thin Film Catalyst Activity Characterization. *Chem. Eng. J.* **2023**, *477*, 146926.

(11) Li, Z.; Öztuna, E.; Skorupska, K.; Vinogradova, O. V.; Jamshaid, A.; Steigert, A.; Rohner, C.; Dimitrakopoulou, M.; Prieto, M. J.; Kunkel, C.; Stredansky, M.; Kube, P.; Götte, M.; Dudzinski, A. M.; Girgsdies, F.; Wrabetz, S.; Frandsen, W.; Blume, R.; Zeller, P.; Muske, M.; Delgado, D.; Jiang, S.; Schmidt, F.-P.; Köhler, T.; Arztmann, M.; Efimenko, A.; Frisch, J.; Kokumai, T. M.; Garcia-Diez, R.; Bär, M.; Hammud, A.; Kröhnert, J.; Trunschke, A.; Scheurer, C.; Schmidt, T.; Lunkenbein, T.; Amkreutz, D.; Kuhlenbeck, H.; Bukas, V. J.; Knop-Gericke, A.; Schlatmann, R.; Reuter, K.; Cuenya, B. R.; Schlögl, R. Rationally Designed Laterally-Condensed-Catalysts Deliver Robust Activity and Selectivity for Ethylene Production in Acetylene Hydrogenation. *Nat. Commun.* **2024**, *15* (1), 10660.

(12) Schäfers, F. The Crystal Monochromator Beamline KMC-1 at BESSY II. *J. Large-Scale Res. Facil. JLSRF* **2016**, *2*, A96.

(13) Lin, H.; Liu, J. X.; Fan, H.-J.; Li, W.-X. Morphology Evolution of FCC and HCP Cobalt Induced by a CO Atmosphere from Ab Initio Thermodynamics. *J. Phys. Chem. C* **2020**, *124*, 23200−23209.

(14) Liu, J.-X.; Su, H.-Y.; Sun, D.-P.; Zhang, B.-Y.; Li, W.-X. Crystallographic Dependence of CO Activation on Cobalt Catalysts: HCP versus FCC. *J. Am. Chem. Soc.* **2013**, *135* (44), 16284−16287.

(15) Tanuma, S.; Powell, C. J.; Penn, D. R. Calculations of Electron Inelastic Mean Free Paths. V. Data for 14 Organic Compounds over the 50−2000 eV Range. *Surf. Interface Anal.* **1994**, *21* (3), 165−176.

(16) Moulder, J. F.; Chastain, J. *Handbook of X-Ray Photoelectron Spectroscopy: A Reference Book of Standard Spectra for Identification and Interpretation of XPS Data*; Physical Electronics Division, Perkin-Elmer Corporation, 1992.

(17) Chuang, T. J.; Brundle, C. R.; Rice, D. W. Interpretation of the X-Ray Photoemission Spectra of Cobalt Oxides and Cobalt Oxide Surfaces. *Surf. Sci.* **1976**, *59* (2), 413−429.
(18) Liu, J.-X.; Su, H.-Y.; Sun, D.-P.; Zhang, B.-Y.; Li, W.-X. Crystallographic Dependence of CO Activation on Cobalt Catalysts: HCP versus FCC. *J. Am. Chem. Soc.* **2013**, *135* (44), 16284−16287.
(19) Zhang, Z.; Nallan, H. C.; Coffey, B. M.; Ngo, T. Q.; Pramanik, T.; Banerjee, S. K.; Ekerdt, J. G. Atomic Layer Deposition of Cobalt Oxide on Oxide Substrates and Low Temperature Reduction to Form Ultrathin Cobalt Metal Films. *J. Vac. Sci. Technol. A* **2019**, *37* (1), 010903.
(20) Kimpel, T. F.; Liu, J.-X.; Chen, W.; Pestman, R.; Hensen, E. J. M. Pressure Dependence and Mechanism of Mn Promotion of Silica-Supported Co Catalyst in the Fischer−Tropsch Reaction. *J. Catal.* **2023**, *425*, 181−195.
(21) Koshy, D. M.; Johnson, G. R.; Bustillo, K. C.; Bell, A. T. Scanning Nanobeam Diffraction and Energy Dispersive Spectroscopy Characterization of a Model Mn-Promoted Co/Al2O3 Nanosphere Catalyst for Fischer−Tropsch Synthesis. *ACS Catal.* **2020**, *10* (20), 12071−12079.
(22) Xue, L.; Han, Y. Inhibition of Dewetting of Thin Polymer Films. *Prog. Mater. Sci.* **2012**, *57* (6), 947−979.
(23) Gavrilović, L.; Jørgensen, E. A.; Pandey, U.; Putta, K. R.; Rout, K. R.; Rytter, E.; Hillestad, M.; Blekkan, E. A. Fischer−Tropsch Synthesis over an Alumina-Supported Cobalt Catalyst in a Fixed Bed Reactor − Effect of Process Parameters. *Catal. Today* **2021**, *369*, 150−157.
(24) Nabaho, D.; Niemantsverdriet, J. W. H.; Claeys, M.; van Steen, E. Hydrogen Spillover in the Fischer−Tropsch Synthesis: An Analysis of Platinum as a Promoter for Cobalt−Alumina Catalysts. *Catal. Today* **2016**, *261*, 17−27.
(25) Mu, S.; Shang, R.; Zhang, J.; Chen, J. Pretreating Co/SiO2 to Generate Highly Active Fischer−Tropsch Synthesis Catalyst with Low CH4 Selectivity. *J. Fuel Chem. Technol.* **2021**, *49* (11), 1592−1597.
(26) Lin, Q.; Liu, B.; Jiang, F.; Fang, X.; Xu, Y.; Liu, X. Assessing the Formation of Cobalt Carbide and Its Catalytic Performance under Realistic Reaction Conditions and Tuning Product Selectivity in a Cobalt-Based FTS Reaction. *Catal. Sci. Technol.* **2019**, *9* (12), 3238−3258.
(27) Kalala, J. Effect of Space Velocity on Fischer−Tropsch Reaction over Co/TiO2 Catalyst. *Proceedings of the World Congress on Engineering and Computer Science*; IAENG, 2015.
(28) Ma, W.; Jacobs, G.; Ji, Y.; Bhatelia, T.; Bukur, D. B.; Khalid, S.; Davis, B. H. Fischer−Tropsch Synthesis: Influence of CO Conversion on Selectivities, H2/CO Usage Ratios, and Catalyst Stability for a Ru Promoted Co/Al2O3 Catalyst Using a Slurry Phase Reactor. *Top. Catal.* **2011**, *54* (13), 757.
(29) Yang, J.; Ma, W.; Chen, D.; Holmen, A.; Davis, B. H. Fischer−Tropsch Synthesis: A Review of the Effect of CO Conversion on Methane Selectivity. *Appl. Catal. Gen.* **2014**, *470*, 250−260.
(30) Claeys, M.; van Steen, E. Chapter 8 - Basic Studies. In *Studies in Surface Science and Catalysis*; Steynberg, A., Dry, M., Eds.; Elsevier, 2004; Vol. *152*, pp 601−680.

https://doi.org/10.1021/acs.iecr.5c02728
Ind. Eng. Chem. Res. 2025, 64, 22939−22948